







Article

Effect of Co, Ti and Cr Additions on Microstructure, Magnetic Properties and Corrosion Resistance of Magnetocaloric Gd-Ge-Si Alloys

Mariusz Hasiak ^{1,*}, Jacek G. Chęćmanowski ², Barbara Kucharska ³, Amadeusz Łaszcz ¹, Aleksandra Kolano-Burian ⁴ and Jerzy Kaleta ¹

¹ Department of Mechanics, Materials and Biomedical Engineering, Wrocław University of Science and Technology, 25 Smoluchowskiego, 50-370 Wrocław, Poland; amadeusz.laszcz@pwr.edu.pl (A.Ł.); jerzy.kaleta@pwr.edu.pl (J.K.)

² Department of Advanced Materials Technologies, Wrocław University of Science and Technology, 25 Smoluchowskiego, 50-370 Wrocław, Poland; jacek.chemanowski@pwr.edu.pl

³ Department of Materials Engineering, Częstochowa University of Technology, 19 Armii Krajowej, 42-200 Częstochowa, Poland; barbara.kucharska@pcz.pl

⁴ Łukasiewicz Research Network, Institute of Non-Ferrous Metals, 5 Sowińskiego, 44-100 Gliwice, Poland; olak@imn.gliwice.pl

* Correspondence: mariusz.hasiak@pwr.edu.pl

Received: 28 November 2020; Accepted: 14 December 2020; Published: 17 December 2020



Abstract: The paper presents studies of microstructure, magnetic and corrosion properties of the $Gd_{58}Ge_{20}Si_{22}$, $Gd_{56}Ge_{20}Si_{22}Co_2$, $Gd_{56}Ge_{20}Si_{22}Ti_2$ and $Gd_{56}Ge_{20}Si_{22}Cr_2$ (at.%) alloys after isothermal heat treatment at 1450 K for 2 h. The structure investigations of the produced materials performed by X-ray diffraction show the presence of $Gd_5Ge_2Si_2$ -type phase in all investigated samples. DC and AC magnetic measurements confirmed that the Curie temperature depends on the chemical composition of the produced alloys. From $M(T)$ characteristics, it was found that the lowest Curie point ($T_C = 268$ K) was estimated for the $Gd_{58}Ge_{20}Si_{22}$ sample, whereas the highest value of the Curie temperature ($T_C = 308$ K) was for the $Gd_{56}Ge_{20}Si_{22}Cr_2$ alloys. Moreover, the GdGeSi alloy without alloying additions shows the highest magnetic entropy change $|\Delta S_M| = 15.07 \text{ J}\cdot\text{kg}^{-1}\cdot\text{K}^{-1}$ for the maximum magnetic field of 2 T. The maximum $|\Delta S_M|$ measured for the $Gd_{56}Ge_{20}Si_{22}$ with the addition of Co, Ti or Cr for the same magnetic field was obtained in the vicinity of the Curie point and equals to 2.92, 2.73 and $2.95 \text{ J}\cdot\text{kg}^{-1}\cdot\text{K}^{-1}$, respectively. Electrochemical studies of the produced materials for 60 min and 55 days exposure in 3% NaCl solution show that the highest stability and corrosion resistance were exhibited the sample with added of Ti.

Keywords: GdGeSi-based alloys; magnetocaloric effect; microstructure; magnetic properties; corrosion resistance

1. Introduction

Rare earth (RE) based alloys are very attractive materials because of their good magnetic properties [1–4]. It has been reported in several papers that materials with the addition of rare earth elements e.g., Gd [5,6], Pr [6–9], Nd [6,10,11], Sm [8], Tb [5] etc. are widely used in many devices, mostly electrical, due to their distinctive thermomagnetic characteristics. When it comes to potential applications in magnetic devices, some of the most interesting materials are Gd-based alloys [12–18]. These alloys are intensively investigated because they exhibit high magnetocaloric effect (MCE), represented by magnetic entropy changed ($|\Delta S_M|$), in the vicinity of the Curie point, which is close to the room temperature [18–20]. It was also shown that the Curie temperature could be

changed by the introduction to master alloys additives such as Co, Fe, Zr, Pr, Ni or Ce [9,16,18,21,22]. High MCE in these alloys allows them to be used in cooling technology, for example, in the production of ecofriendly magnetic refrigerators [23–27]. The possibilities of increasing magnetocaloric effect in RE-based materials by proper heat treatment and/or chemical composition changes, together with reducing hysteresis loss [28–31] and improving application properties, such as corrosion resistance and stability [15,32–34] as well as mechanical properties [35–37], is one of the most important issues in research on these alloys.

The aim of this paper is to study the effect of Co, Ti and Cr addition on microstructure, DC and AC thermomagnetic properties as well as corrosion stability and resistivity for the $Gd_{58-x}Ge_{20}Si_{22}Y_x$ ($x = 0$ or 2 ; $Y = Co, Ti$ or Cr) alloys after the heat treatment at 1450 K for 2 h. Particular attention in this work is devoted to the influence of additives on the Curie temperature change, which is essential from the application point of view. The introduction of Co, Ti and Cr atoms to master GdGeSi alloy, besides influence on microstructure and thermomagnetic properties, changes electrochemical properties. The main reason for using the alloying additives stems from the fact that in the presence of Cr, the oxidation resistance of metallic materials increases, which leads to the creation of a dense oxide layer and limits the rate of corrosion processes. A similar effect is also observed in Co- and Ti-containing alloys.

2. Materials and Methods

GdGeSi-based alloys with additions of Co, Ti or Cr and a nominal compositions of $Gd_{58}Ge_{20}Si_{22}$, $Gd_{56}Ge_{20}Si_{22}Co_2$, $Gd_{56}Ge_{20}Si_{22}Ti_2$ and $Gd_{56}Ge_{20}Si_{22}Cr_2$ (at.%) were produced with the help of an arc melter system in an argon atmosphere using high-purity elements. The total mass of the produced samples was about 10 g. The ingots were remelted five times in order to achieve a homogeneous structure. All samples were subjected to isothermal annealing at 1450 K for 2 h. The temperature for the heat treatment process was chosen according to differential scanning calorimetry (DSC) measurements. The phase composition of the $Gd_{58-x}Ge_{20}Si_{22}Y_x$ alloys, where $x = 0$ or 2 and $Y = Co, Ti$ or Cr , was examined by X-ray diffraction (XRD) with the help of a Seifert 3003TT diffractometer (Seifert, Mannheim, Germany) working in Bragg–Brentano geometry for $CoK_{\alpha} = 0.17902$ nm radiation in the angle range $2\Theta = 35\text{--}55^\circ$ for the samples in the form of powders. The structure studies and chemical composition analysis of the produced materials were performed by both optical microscopy and scanning electron microscopy equipped with an energy dispersive X-ray spectroscopy (SEM, Quanta 250, FEI, Thermo Fisher Scientific, Waltham, MA, USA) detector working in secondary electrons (SE) mode. Thermomagnetic measurements, i.e., magnetization and magnetic susceptibility versus temperature for the $Gd_{58}Ge_{20}Si_{22}$ as well as Co-, Ti- and Cr-containing samples, were carried out by the Versalab and Physical Property Measurement System (PPMS, Quantum Design, San Diego, CA, USA) to determine the Curie point ($M(T)$ characteristics recorded at the external magnetic field of 0.25 T) and magnetocaloric effect (MCE) described as magnetic entropy changes (ΔS_M). DC magnetic measurements (temperature dependence of magnetization, sets of isothermal magnetization curves) were performed at temperature range 50–400 K and extremal magnetic field up to 2 T. AC magnetic susceptibility (ACMS) was recorded from 50 to 350 K for excitation magnetic field of 0.5 mT and frequency of 100 Hz at zero external DC magnetic field. Corrosion resistance tests were conducted in 3% NaCl solution for 60 min and 55 days. DC electrochemical measurements were conducted by recording polarization curves in the conventional three-electrode system. The measuring setup included a measuring vessel and Schlumberger SI 1286 potentiostat (Ametek, Berwyn, PA, USA). The measurements started from the potential of -350 mV in the anode direction with a rate of 1 mV/s.

3. Results and Discussion

3.1. Structure and Phase Investigations of the $Gd_{58-x}Ge_{20}Si_{22}Y_x$ ($x = 0$ or 2 ; $Y = Co, Ti$ or Cr) Alloys

The investigation of microstructure performed with the help of X-ray diffractometer for the $Gd_{58-x}Ge_{20}Si_{22}Y_x$ ($x = 0$ or 2 ; $Y = Co, Ti$ or Cr) alloys after isothermal annealing at 1450 K for 2 h is presented in Figure 1. It can be seen that diffraction pattern recorded for diffraction angle $2\theta = 35\text{--}55^\circ$ for all investigated materials shows the presence of peaks, which can be assigned to the required high magnetocaloric $Gd_5Ge_2Si_2$ -type phase. The changes in the intensity of peaks between investigated samples reflect additions of Co, Ti and Cr to master $Gd_{58}Ge_{20}Si_{22}$ alloy and texture of the examined materials. It is particularly evident for the reflex described by d-spacing in Bragg's law equals to $d_{hkl} = 2.68 \text{ \AA}$ for the (0 4 2) plane (PDF cards: 04-008-5158 or 01-073-3500).

The microstructure and phase composition studies of the produced materials performed by an optical microscope and an SEM in SE mode equipped with an EDS detector are presented in Figure 2. The micrographs of the $Gd_{58}Ge_{20}Si_{22}$, $Gd_{56}Ge_{20}Si_{22}Co_2$, $Gd_{56}Ge_{20}Si_{22}Ti_2$ and $Gd_{56}Ge_{20}Si_{22}Cr_2$ recorded with the help of OM (Figure 2, left column) show the presence of dendrites with different sizes precipitated during the annealing process. The images of fracture of the $Gd_{58-x}Ge_{20}Si_{22}Y_x$ ($x = 0$ or 2 ; $Y = Co, Ti$ or Cr) alloys obtained from SEM/SE presented in the middle column in Figure 2 shows no significant changes between investigated samples and suggests similar brittleness of the produced materials despite the noticeable difference in the microstructure. The investigations of chemical composition for all samples performed by SEM with EDS analysis were conducted to confirm the nominal 5:2:2 ratio for the Gd:Ge:Si phase. The obtained results are in good agreement with X-ray examination data. Moreover, the presence of alloying additions such as Co, Ti and Cr in GdGeSi-based alloy is evident as additional peaks on the EDS spectra (Figure 2, right column).

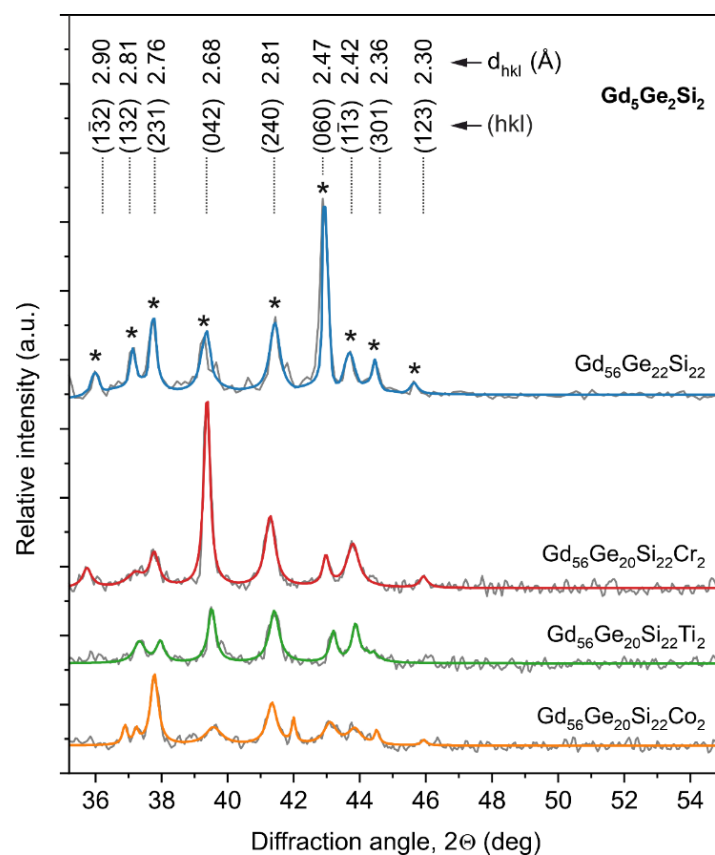


Figure 1. X-ray diffraction pattern of the $Gd_{58-x}Ge_{20}Si_{22}Y_x$ ($x = 0$ or 2 ; $Y = Co, Ti$ or Cr) alloys after heat treatment at 1450 K for 2 h. The peaks corresponding to $Gd_5Ge_2Si_2$ -type phase are marked with an asterisk.

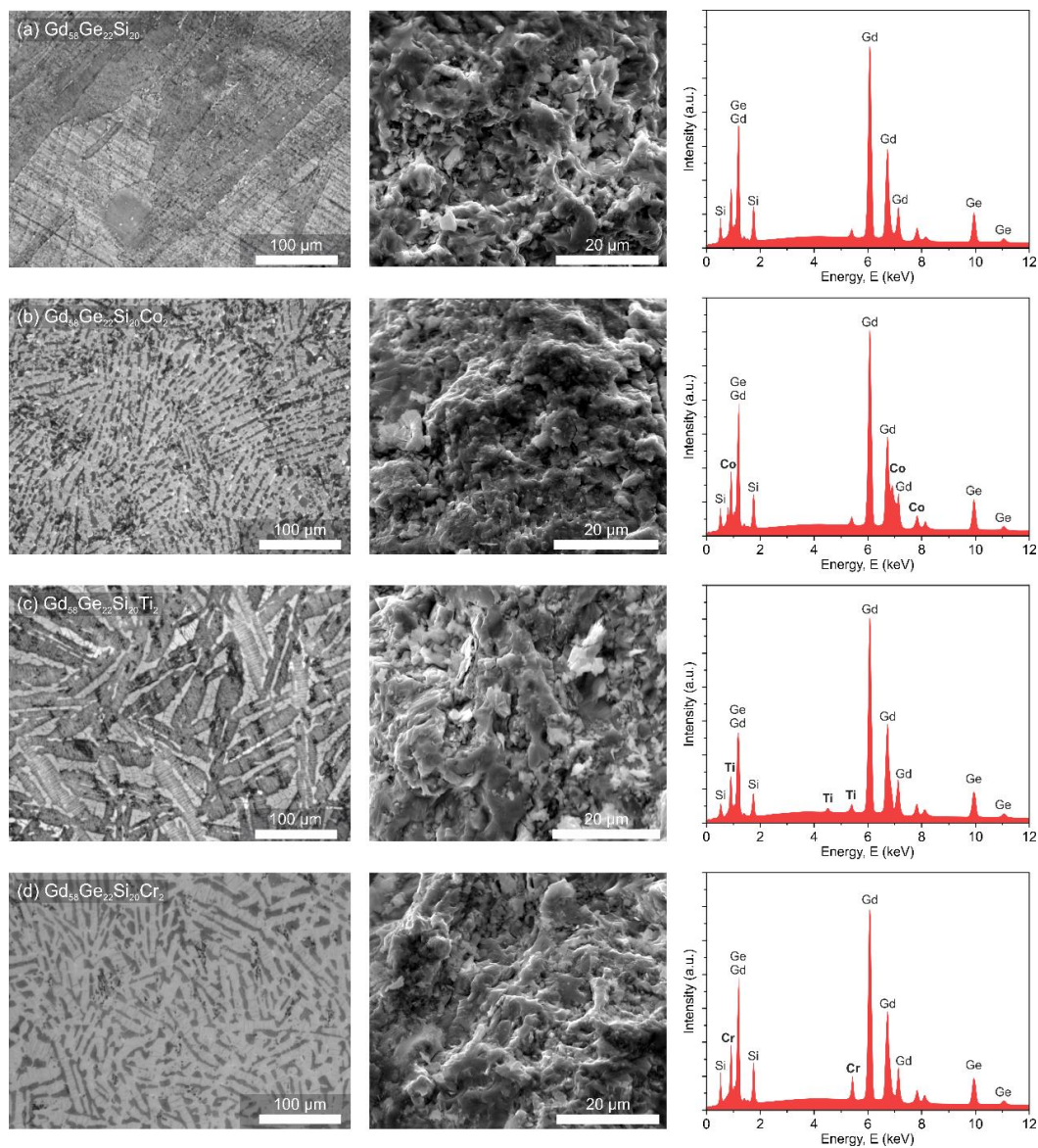


Figure 2. Optical microscopy images (left column), SEM/SE fracture images (middle column) and corresponding EDS spectra (right column) for the annealed $\text{Gd}_{58}\text{Ge}_{20}\text{Si}_{22}$ (a), $\text{Gd}_{56}\text{Ge}_{20}\text{Si}_{22}\text{Co}_2$ (b), $\text{Gd}_{56}\text{Ge}_{20}\text{Si}_{22}\text{Ti}_2$ (c) and $\text{Gd}_{56}\text{Ge}_{20}\text{Si}_{22}\text{Cr}_2$ (d) alloys.

3.2. Magnetic Properties of GdGeSi Alloy without and with the Addition of Co, Ti and Cr

Figure 3 (left side) shows the temperature dependence of magnetization ($M(T)$) for the annealed $\text{Gd}_{58-x}\text{Ge}_{20}\text{Si}_{22}\text{Y}_x$ ($x = 0$ or 2 ; $\text{Y} = \text{Co}, \text{Ti}$ or Cr) alloys performed with a heating rate of 10 K/min in zero field-cooled mode at the external magnetic field of 0.25 T recorded in the temperature range $50\text{--}400 \text{ K}$.

The Curie point (T_C) for all analyzed samples calculated as a temperature, which corresponds to the minimum value of the derivative dM/dT , is presented in Figure 3 (right side). The recorded $M(T)$ thermomagnetic characteristics are typical for ferromagnetic materials with first (FOPT) and second (SOPT) order phase transition. The $\text{Gd}_{58}\text{Ge}_{20}\text{Si}_{22}$ sample shows the lower Curie point ($T_C = 268 \text{ K}$) in comparison to sample with the addition of Co, Ti and Cr (304 K , 298 K and 308 K , respectively). The addition $2 \text{ at.}\%$ of Co, Ti or Cr to master GdGeSi alloy leads to an increase of the Curie point, which is important from the application point of view. On the other hand, the magnetic magnetization measured at the same temperature in the ferromagnetic region ($50\text{--}250 \text{ K}$) varies with the chemical composition of produced materials. The $\text{Gd}_{58}\text{Ge}_{20}\text{Si}_{22}$ sample exhibits higher magnetization than samples with additives (Figure 3). Moreover, the reference GdGeSi sample shows FOTP [16], whereas Co-, Ti and

Cr-containing materials present ferromagnetic to paramagnetic phase transition described as SOPT. It is worth noting that the smallest value of M in the temperature range 50–250 K for all investigated samples was observed for the Co-containing sample despite the highest magnetic moment.

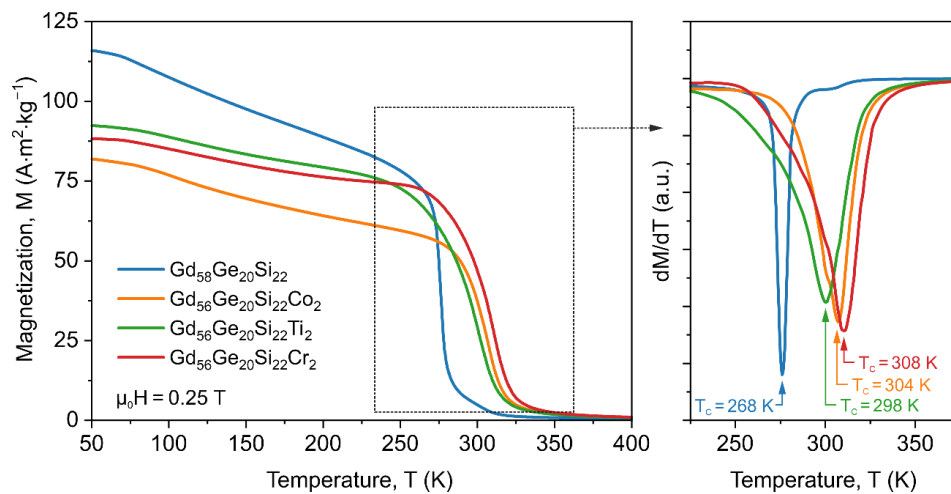


Figure 3. Magnetic magnetization versus temperature curves for the $\text{Gd}_{58}\text{Ge}_{20}\text{Si}_{22}$, $\text{Gd}_{56}\text{Ge}_{20}\text{Si}_{22}\text{Co}_2$, $\text{Gd}_{56}\text{Ge}_{20}\text{Si}_{22}\text{Ti}_2$ and $\text{Gd}_{56}\text{Ge}_{20}\text{Si}_{22}\text{Cr}_2$ alloys annealed at 1450 K for 2 h recorded at external DC magnetic field of 0.25 T.

The estimation of the Curie temperature for the annealed GdGeSi-based alloys with the addition of Co, Ti and Cr was also performed by registering AC magnetic susceptibility versus temperature for the excitation magnetic field of 0.5 mT, without an external magnetic field (Figure 4). It is clear that the values of the Curie point are in good agreement with the results obtained from $M(T)$ analysis and the Curie temperature for the $\text{Gd}_{58}\text{Ge}_{20}\text{Si}_{22}$, $\text{Gd}_{56}\text{Ge}_{20}\text{Si}_{22}\text{Co}_2$, $\text{Gd}_{56}\text{Ge}_{20}\text{Si}_{22}\text{Ti}_2$ and $\text{Gd}_{56}\text{Ge}_{20}\text{Si}_{22}\text{Cr}_2$ alloys equals to 267 K, 304 K, 297 K and 307 K, respectively. The difference between the Curie points obtained from magnetization and ACMS versus temperature measurements are due to the external magnetic field, which was applied only during $M(T)$ investigations. It is also worth noting that on the AC magnetic susceptibility versus temperature curves just below the Curie point the Hopkinson peak for Ti- and Cr-containing sample was observed. This effect seems to be due to the incoherent rotation of the magnetization during the reversal process when AC excitation magnetic field is applied [38].

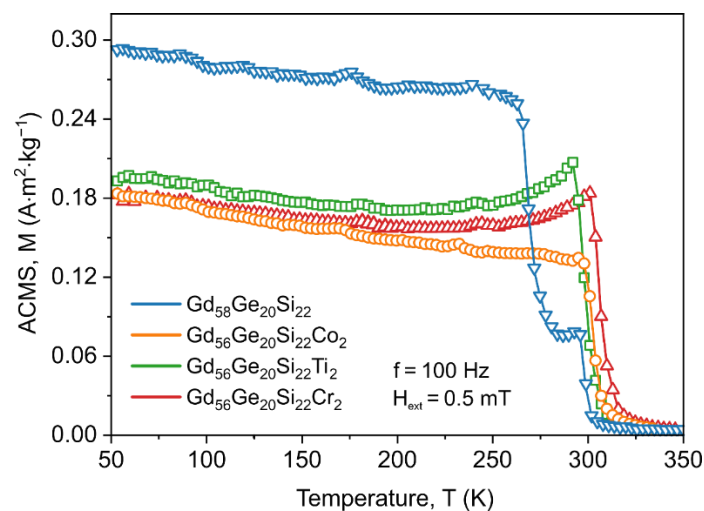


Figure 4. Temperature dependence of AC magnetic susceptibility (ACMS) for the annealed $\text{Gd}_{58}\text{Ge}_{20}\text{Si}_{22}$, $\text{Gd}_{56}\text{Ge}_{20}\text{Si}_{22}\text{Co}_2$, $\text{Gd}_{56}\text{Ge}_{20}\text{Si}_{22}\text{Ti}_2$ and $\text{Gd}_{56}\text{Ge}_{20}\text{Si}_{22}\text{Cr}_2$ alloys measured at zero external magnetic field for the excitation AC magnetic field of 0.5 mT and frequency of 100 Hz.

Figure 5 presents the set of isothermal $M(\mu_0H)$ curves (left column) and corresponding magnetic entropy effect investigations (right column) for the annealed $Gd_{58-x}Ge_{20}Si_{22}Y_x$ ($x = 0$ or 2 ; $Y = Co, Ti$ or Cr). MCE is described as isothermal magnetic entropy change (ΔS_M) and can be calculated according to Maxwell’s thermomagnetic relation [39]:

$$\Delta S_M = \mu_0 \int_0^{H_m} \left(\frac{\partial M(T, H)}{\partial T} \right)_H dH = \int_0^{B_m} \frac{\partial M(T, H)}{\partial T} dB \tag{1}$$

where $B_m = \mu_0 H_m$. The changes of magnetic entropy (ΔS_M) versus temperature were calculated from the sets of isothermal magnetization curves (Figure 5, left column), recorded for maximum magnetizing field up to 2 T, using numerical approximation described by the equation:

$$|\Delta S_M| = \sum_i \frac{1}{T_{i+1} - T_i} (M_i - M_{i+1})_H \Delta H_i \tag{2}$$

where M_i and M_{i+1} are magnetizations measured for magnetizing field H at temperatures T_i and T_{i+1} , respectively.

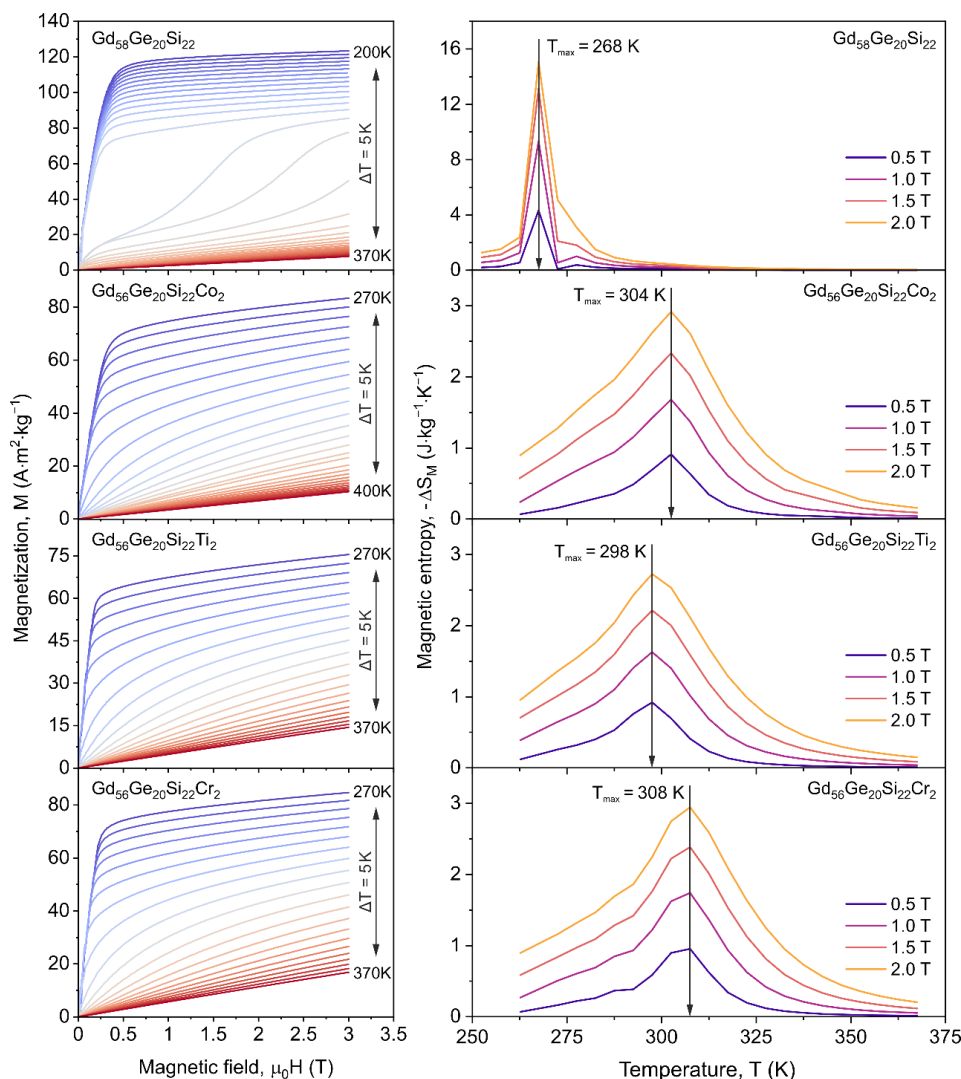


Figure 5. Set of isothermal $M(\mu_0H)$ curves and corresponding magnetic entropy changes versus temperature calculated for the $Gd_{58-x}Ge_{20}Si_{22}Y_x$ ($x = 0$ or 2 ; $Y = Co, Ti$ or Cr) alloys at the maximum external magnetizing field of 0.5 T, 1.0 T, 1.5 T and 2.0 T.

$M(\mu_0H)$ characteristics recorded in the vicinity of the Curie point (Figure 5 left column) confirm the FOPT in the $Gd_{58}Ge_{20}Si_{22}$ and SOPT in the $Gd_{56}Ge_{20}Si_{22}Y_2$ ($Y = Co, Ti$ or Cr). The increase of magnetizing field from 0.5 T to 2 T leads to increase of the maximum value of $|\Delta S_M|$ from 4.33 to $15.07 J \cdot kg^{-1} \cdot K^{-1}$, from 0.91 to $2.92 J \cdot kg^{-1} \cdot K^{-1}$, from 0.92 to $2.73 J \cdot kg^{-1} \cdot K^{-1}$ and from 0.96 to $2.95 J \cdot kg^{-1} \cdot K^{-1}$ for the $Gd_{58}Ge_{20}Si_{22}$, $Gd_{56}Ge_{20}Si_{22}Co_2$, $Gd_{56}Ge_{20}Si_{22}Ti_2$ and $Gd_{56}Ge_{20}Si_{22}Cr_2$ alloys, respectively. Moreover, the maximum on $-\Delta S_M(T)$ characteristics was observed close to the Curie point of the investigated materials. Obtained results revealed in Figure 5 suggest that the addition of Co, Ti or Cr atoms to GdGeSi-based alloy drastically reduce $|\Delta S_M|$. Moreover, Co-, Ti- and Cr-containing samples present near to Curie point almost the same maximum values of magnetocaloric effect, which are more than five times lower than for the $Gd_{58}Ge_{20}Si_{22}$ alloy. The similar thermomagnetic behaviour was also reported for the magnetocaloric Gd-based alloys doped by a different alloying element such as Zr, Mn, Tb, Fe [9,12,16,18,22].

3.3. Corrosion Properties of GdGeSi-Based Alloys

Due to the good corrosion resistance of Co, Ti and Cr, the influence of these additives on the corrosion behavior of the $Gd_{58-x}Ge_{20}Si_{22}Y_x$ ($x = 0$ or 2 ; $Y = Co, Ti$ or Cr) alloys was investigated. From an application point of view, the corrosion resistance of the investigated magnetocaloric materials is significant because these alloys usually work in chloride-containing water used as a cooling medium in environmentally friendly refrigeration. All investigations of electrochemical properties presented below were performed for the Co-, Ti- and Cr-containing samples in relation to the $Gd_{58}Ge_{20}Si_{22}$ as the reference sample. Figures 6 and 7 present the corrosion properties of the investigated alloys after 60 min. and 55 days exposition in 3% NaCl solution, respectively. Figure 6 shows that for the $Gd_{58}Ge_{20}Si_{22}$ sample and with the addition of Co, Ti and Cr, even for a short exposure time (60 min. in 3% NaCl solution), differences in the rates of the electrode processes proceeding on the metallic surface were registered.

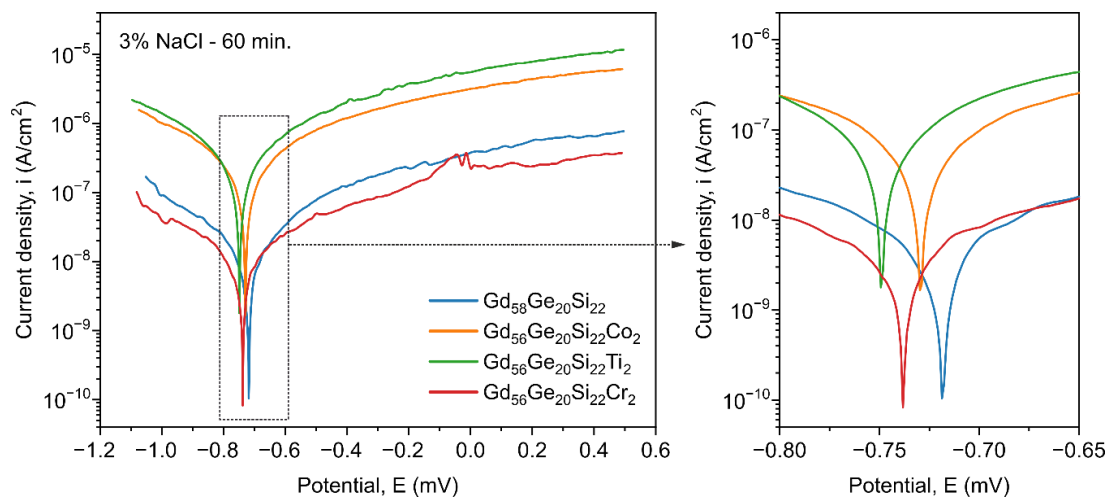


Figure 6. Polarisation curves determined in 3% NaCl solution for the $Gd_{58-x}Ge_{20}Si_{22}Y_x$ ($x = 0$ or 2 ; $Y = Co, Ti$ or Cr) alloys after 60 min exposure.

The electrode processes proceed the slowest, in both the anode region and the cathode region, on the surface of Ti-containing sample. The presence of Co and Cr in the GdGeSi alloys causes the electrode processes to proceed more easily than in the case of the metallic substrate without the alloy additions. This is due to the difference in passivation presented by Co, Ti and Cr. Among the used alloying elements, Ti shows the strongest tendency towards surface passivation. The presence of Co, Ti and Cr in the matrix of the GdGeSi alloy does not show a significant effect on the values of the particular electrochemical parameters (Table 1). After 60 min exposure in the corrosive solution, the maximum differences between the corrosion potential (E_{corr}) values of 44 mV and the cathodic–anodic transition

potential (E_{C-A}) values of 28 mV were measured for the $Gd_{56}Ge_{20}Si_{22}Cr_2$ and $Gd_{58}Ge_{20}Si_{22}$ alloys (Table 1). The highest polarization resistance ($R_p = 4.18 \times 10^6 \Omega \cdot cm^2$) and the lowest rate of corrosion ($i_{corr} = 6.23 \times 10^{-9} A/cm^2$) were recorded for the $Gd_{56}Ge_{20}Si_{22}Ti_2$ alloy. The rate of corrosion for this material is about 15 times lower than for the Cr-containing material. Moreover, the $Gd_{56}Ge_{20}Si_{22}Ti_2$ and $Gd_{58}Ge_{20}Si_{22}$ alloys present comparable corrosion resistance. On the basis of the obtained data, it can be concluded that the $Gd_{56}Ge_{20}Si_{22}Ti_2$ alloy after 60 min exposure in 3% NaCl solution presents the highest corrosion resistance, whereas the $Gd_{56}Ge_{20}Si_{22}Cr_2$ alloy exhibits the lowest corrosion resistance.

The long-time (55 days) exposure in 3% NaCl solution for the $Gd_{58-x}Ge_{20}Si_{22}Y_x$ ($x = 0$ or 2 ; $Y = Co, Ti$ or Cr) alloys leads to the significant differences in the rates of the electrode processes in both the cathode and anode region in comparison to 60 min exposure in the same solution (Figure 7, Table 1). Taking into account the obtained values of polarization resistance and rates of corrosion for all investigated samples (55 days exposure time), the $Gd_{58}Ge_{20}Si_{22}$ and $Gd_{56}Ge_{20}Si_{22}Ti_2$ alloys show the highest (in comparison to samples with Co and Cr) and comparable corrosion resistance. The resulting passive layer of titanium oxide effectively limits the rate of electrode processes in the anode area and does not tend to allow pitting corrosion (as in the case of an alloy containing Co or Cr).

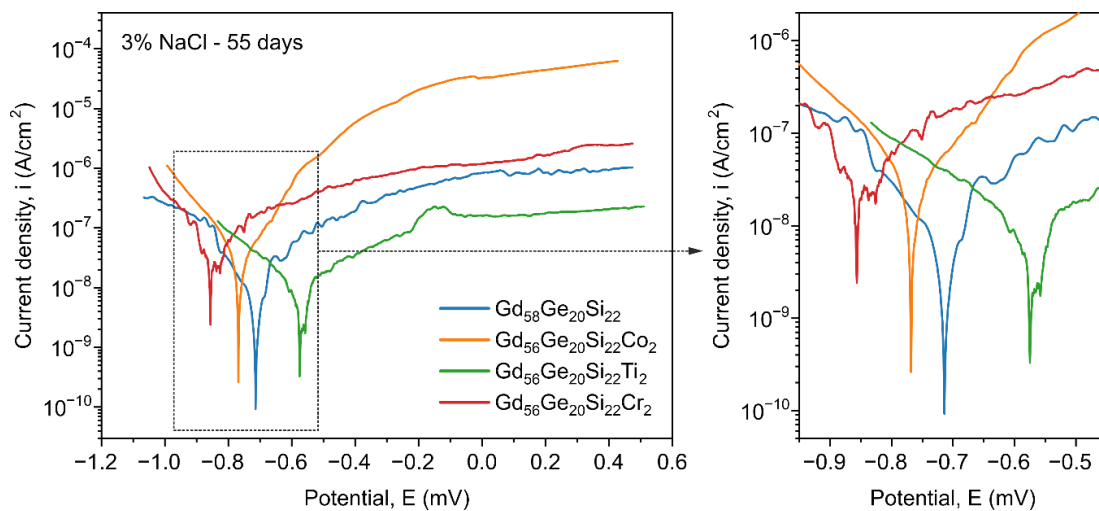


Figure 7. Polarisation curves determined in 3% NaCl solution for the the $Gd_{58-x}Ge_{20}Si_{22}Y_x$ ($x = 0$ or 2 ; $Y = Co, Ti$ or Cr) alloys after 55 days exposure.

Table 1. Corrosion potential (E_{corr}), cathodic to anodic transition potential (E_{C-A}), polarization resistance (R_p) and corrosion current density (i_{corr}) for the $Gd_{58}Ge_{20}Si_{22}$, $Gd_{56}Ge_{20}Si_{22}Co_2$, $Gd_{56}Ge_{20}Si_{22}Ti_2$ and $Gd_{56}Ge_{20}Si_{22}Cr_2$ alloys in 3% NaCl solutions after two exposure times.

Time of Exposition	Alloy	E_{corr} (mV)	E_{C-A} (mV)	R_p ($\Omega \cdot cm^2$)	i_{corr} (A/cm^2)
60 min	$Gd_{58}Ge_{20}Si_{22}$	-707	-720	3.46×10^6	7.54×10^{-9}
	$Gd_{56}Ge_{20}Si_{22}Co_2$	-729	-729	2.90×10^5	8.98×10^{-8}
	$Gd_{56}Ge_{20}Si_{22}Ti_2$	-737	-737	4.18×10^6	6.26×10^{-9}
	$Gd_{56}Ge_{20}Si_{22}Cr_2$	-751	-748	2.27×10^5	1.15×10^{-7}
55 days	$Gd_{58}Ge_{20}Si_{22}$	-721	-713	3.56×10^6	7.33×10^{-9}
	$Gd_{56}Ge_{20}Si_{22}Co_2$	-647	-766	7.49×10^5	3.48×10^{-8}
	$Gd_{56}Ge_{20}Si_{22}Ti_2$	-487	-571	3.62×10^6	7.21×10^{-9}
	$Gd_{56}Ge_{20}Si_{22}Cr_2$	-704	-855	5.06×10^5	5.15×10^{-8}

For the $Gd_{58-x}Ge_{20}Si_{22}Y_x$ ($x = 0$ or 2 ; $Y = Co, Ti$ or Cr) alloys the best stability and corrosion resistance after 55 days exposition in the 3% NaCl solution are presented by the Ti-containing alloy. This material shows the highest values of $E_{corr} = -487$ mV and $E_{C-A} = -571$ mV in comparison to other investigated alloys. Moreover, the polarization resistance (R_p) and current corrosion density (i_{corr}) for

Ti-containing sample are comparable with data measured for the $Gd_{58}Ge_{20}Si_{22}$ alloys (Table 1). It is also clear that the $Gd_{56}Ge_{20}Si_{22}Co_2$ and $Gd_{56}Ge_{20}Si_{22}Cr_2$ alloys show similar corrosion properties; however, they are much worse than the $Gd_{56}Ge_{20}Si_{22}Ti_2$ and $Gd_{58}Ge_{20}Si_{22}$ materials. From electrochemical investigations presented above (Figures 6 and 7, Table 1) it can be concluded that relatively the highest stability and corrosion resistance in 3% NaCl solution are shown by the sample with the addition of Ti.

4. Conclusions

The paper presents the influence of Co, Ti and Cr additions to GdGeSi-based alloy on the Curie temperature change, magnetocaloric effect as well as corrosion stability for the $Gd_{58-x}Ge_{20}Si_{22}Y_x$ ($x = 0$ or 2; $Y = Co, Ti$ or Cr) alloys. X-ray diffraction shows the presence of master $Gd_5Ge_2Si_2$ -type phase in all investigated samples. The additional SEM/EDS analysis confirms the presence of Co, Ti and Cr in GdGeSi-based alloy as well as the nominal 5:2:2 ratio for the Gd:Ge:Si phase. From an application point of view all additives studied in this paper increase the Curie point from $T_C = 268$ K for the $Gd_{58}Ge_{20}Si_{22}$ alloy to temperatures which are close to room temperature, i.e., 304 K, 298 K and 308 K for the Co-, Ti and Cr-containing alloys, respectively. The magnetocaloric effect, described as the maximum magnetic entropy change, observed near the Curie point strongly depends on chemical composition and, for the $Gd_{58}Ge_{20}Si_{22}$ sample ($|\Delta S_M| = 15.07 \text{ J}\cdot\text{kg}^{-1}\cdot\text{K}^{-1}$), is more than five times higher than for the materials with 2 at.% addition of Co, Ti and Cr (2.92, 2.73 and $2.95 \text{ J}\cdot\text{kg}^{-1}\cdot\text{K}^{-1}$, respectively). On the other hand, it should be noted that this lower MCE in doped alloys occurs in the vicinity of the room temperature and is still valuable from an application point of view. Moreover, the electrochemical data shows an improvement of corrosion resistance for all doped materials in comparison to the main $Gd_{58}Ge_{20}Si_{22}$ alloy. It is worth noting that the best corrosion resistance in 3% NaCl solution was observed for the Ti-containing sample. The same $Gd_{56}Ge_{20}Si_{22}Ti_2$ alloy exhibits the strongest tendency towards surface passivation during both 60 min and 55 days of exposure (polarization resistance of $4.18 \times 10^6 \Omega\cdot\text{cm}^2$ and $3.62 \times 10^6 \Omega\cdot\text{cm}^2$ as well as corrosion current density of $6.26 \times 10^{-9} \text{ A/cm}^2$ and $7.21 \times 10^{-9} \text{ A/cm}^2$, respectively).

Author Contributions: Conceptualization, M.H., J.G.C. and B.K.; methodology, M.H., J.G.C. and B.K.; formal analysis, M.H., J.G.C., B.K. and A.L.; investigation, M.H., J.G.C., B.K. and A.K.-B.; data curation, M.H., J.G.C., B.K. and A.L.; writing—original draft preparation, M.H., J.G.C., B.K. and A.L.; writing—review and editing, M.H., J.G.C., B.K., A.L., A.K.-B. and J.K.; visualization, M.H., J.G.C., B.K. and A.L.; supervision, J.K. All authors have read and agreed to the published version of the manuscript.

Funding: This research received no external funding.

Acknowledgments: We would like to acknowledge Dajana Pluta for her assistance and help in sample preparation and microstructure investigations.

Conflicts of Interest: The authors declare no conflict of interest.

References

1. Elliott, R.J. *Magnetic Properties of Rare Earth Metals*; Elliott, R.J., Ed.; Springer: Boston, MA, USA, 1972; ISBN 978-1-4757-5693-7.
2. Luo, Q.; Wang, W.H. Magnetocaloric effect in rare earth-based bulk metallic glasses. *J. Alloys Compd.* **2010**, *495*, 209–216. [[CrossRef](#)]
3. Gutfleisch, O.; Willard, M.A.; Brück, E.; Chen, C.H.; Sankar, S.G.; Liu, J.P. Magnetic Materials and Devices for the 21st Century: Stronger, Lighter, and More Energy Efficient. *Adv. Mater.* **2011**, *23*, 821–842. [[CrossRef](#)]
4. Phan, M.H.; Yu, S.C. Review of the magnetocaloric effect in manganite materials. *J. Magn. Magn. Mater.* **2007**, *308*, 325–340. [[CrossRef](#)]
5. Chrobak, A.; Nosenko, V.; Haneczok, G.; Boichyshyn, L.; Kotur, B.; Bajorek, A.; Zivotsky, O.; Hendrych, A. Effect of rare earth additions on magnetic properties of $Fe_{82}Nb_2B_{14}RE_2$ ($RE = Y, Gd, Tb$ and Dy) amorphous alloys. *Mater. Chem. Phys.* **2011**, *130*, 603–608. [[CrossRef](#)]
6. Xiao, S.; Chen, Y. Magnetic properties and magnetic exchange interactions in $Gd_{1-x}RE_x$ ($RE = Pr, Nd$) alloys. *J. Rare Earths* **2016**, *34*, 489–494. [[CrossRef](#)]

7. Zhao, L.; Tian, X.; Yao, Z.; Zhao, X.; Wang, R.; Hamt, O.; Jiang, L.; Harris, V.G. Enhanced magnetostrictive properties of lightly Pr-doped Fe₈₃Ga₁₇ alloys. *J. Rare Earths* **2020**, *38*, 257–264. [[CrossRef](#)]
8. Aryal, A.; Quetz, A.; Pandey, S.; Dubenko, I.; Stadler, S.; Ali, N. Magnetocaloric effects and transport properties of rare-earth (R = La, Pr, Sm) doped Ni_{50-x}R_xMn₃₅Sn₁₅ Heusler alloys. *J. Alloys Compd.* **2017**, *717*, 254–259. [[CrossRef](#)]
9. Hasiak, M.; Łaszcz, A. Microstructure to thermomagnetic and mechanical properties relationship in Gd₇₅Ge₁₅Si₅Pr₅ alloy. *J. Rare Earths* **2019**, *37*, 1213–1217. [[CrossRef](#)]
10. Naik, S.R.; Salker, A.V. Change in the magnetostructural properties of rare earth doped cobalt ferrites relative to the magnetic anisotropy. *J. Mater. Chem.* **2012**, *22*, 2740–2750. [[CrossRef](#)]
11. Dent, P.C. Rare earth elements and permanent magnets (invited). *J. Appl. Phys.* **2012**, *111*, 07A721. [[CrossRef](#)]
12. Yüzüak, E.; Dincer, I.; Elerman, Y. Effects of manganese doping on magnetocaloric effect in Ge-rich Gd₅Ge_{2.05}Si_{1.95} alloy. *J. Rare Earths* **2012**, *30*, 217–221. [[CrossRef](#)]
13. Bingham, N.S.; Wang, H.; Qin, F.; Peng, H.X.; Sun, J.F.; Franco, V.; Srikanth, H.; Phan, M.H. Excellent magnetocaloric properties of melt-extracted Gd-based amorphous microwires. *Appl. Phys. Lett.* **2012**, *101*, 102407. [[CrossRef](#)]
14. Pecharsky, V.K.; Gschneidner, K.A., Jr. Giant magnetocaloric effect in Gd₅(Si₂Ge₂). *Phys. Rev. Lett.* **1997**, *78*, 4494. [[CrossRef](#)]
15. Zhong, X.; Shen, X.; Liu, Z. Magnetocaloric properties, microhardness and corrosion resistance of Gd_{100-x}Zr_x alloys. *J. Rare Earths* **2016**, *34*, 889–894. [[CrossRef](#)]
16. Hasiak, M. Microstructure and magnetocaloric effect in as-quenched GdGeSi alloys with addition of Ni and Ce. *Phys. Status Solidi Appl. Mater. Sci.* **2016**, *213*, 1130–1137. [[CrossRef](#)]
17. Belo, J.H.; Pereira, A.M.; Ventura, J.; Oliveira, G.N.P.; Araújo, J.P.; Tavares, P.B.; Fernandes, L.; Algarabel, P.A.; Magen, C.; Morellon, L.; et al. Phase control studies in Gd₅Si₂Ge₂ giant magnetocaloric compound. *J. Alloys Compd.* **2012**, *529*, 89–95. [[CrossRef](#)]
18. Zhang, T.; Chen, Y.; Tang, Y.; Du, H.; Ren, T.; Tu, M. The phase formation and thermal hysteresis of Gd₅Si₂Ge₂ with the addition of transition elements (Mn, Fe, Co, Ni). *J. Alloys Compd.* **2007**, *433*, 18–21. [[CrossRef](#)]
19. Franco, V.; Blázquez, J.S.; Ingale, B.; Conde, A. The magnetocaloric effect and magnetic refrigeration near room temperature: Materials and models. *Annu. Rev. Mater. Res.* **2012**, *42*, 305–342. [[CrossRef](#)]
20. Xu, L.; Qian, C.; Ai, Y.; Su, T.; Hou, X. Tunable Magnetocaloric Properties of Gd-Based Alloys by Adding Tb and Doping Fe Elements. *Materials* **2019**, *12*, 2877. [[CrossRef](#)]
21. Ferenc, J.; Kowalczyk, M.; Cieślak, G.; Erenc-Śędziak, T.; Kulik, T. Improvement of magnetocaloric properties of Gd-Ge-Si alloys by alloying with iron. *EPJ Web Conf.* **2013**, *40*, 3–6. [[CrossRef](#)]
22. Prabahar, K.; Raj Kumar, D.M.; Manivel Raja, M.; Chandrasekaran, V. Phase analysis and magnetocaloric properties of Zr substituted Gd-Si-Ge alloys. *J. Magn. Magn. Mater.* **2011**, *323*, 1755–1759. [[CrossRef](#)]
23. Brück, E. Developments in magnetocaloric refrigeration. *J. Phys. D Appl. Phys.* **2005**, *38*. [[CrossRef](#)]
24. Kitanovski, A. Energy Applications of Magnetocaloric Materials. *Adv. Energy Mater.* **2020**, *10*. [[CrossRef](#)]
25. Lyubina, J. Magnetocaloric materials for energy efficient cooling. *J. Phys. D Appl. Phys.* **2017**, *50*. [[CrossRef](#)]
26. Tishin, A.M.; Spichkin, Y.I. Recent progress in magnetocaloric effect: Mechanisms and potential applications. *Int. J. Refrig.* **2014**, *37*, 223–229. [[CrossRef](#)]
27. Waske, A.; Gruner, M.E.; Gottschall, T.; Gutfleisch, O. Magnetocaloric materials for refrigeration near room temperature. *MRS Bull.* **2018**, *43*, 269–273. [[CrossRef](#)]
28. Gutfleisch, O.; Gottschall, T.; Fries, M.; Benke, D.; Radulov, I.; Skokov, K.P.; Wende, H.; Gruner, M.; Acet, M.; Entel, P.; et al. Mastering hysteresis in magnetocaloric materials. *Philos. Trans. R. Soc. A Math. Phys. Eng. Sci.* **2016**, *374*. [[CrossRef](#)]
29. Scheibel, F.; Gottschall, T.; Taubel, A.; Fries, M.; Skokov, K.P.; Terwey, A.; Keune, W.; Ollefs, K.; Wende, H.; Farle, M.; et al. Hysteresis Design of Magnetocaloric Materials—From Basic Mechanisms to Applications. *Energy Technol.* **2018**, *6*, 1397–1428. [[CrossRef](#)]
30. Basso, V.; Piazzini, M.; Bennati, C.; Curcio, C. Hysteresis and Phase Transition Kinetics in Magnetocaloric Materials. *Phys. Status Solidi Basic Res.* **2018**, *255*, 1700278. [[CrossRef](#)]
31. Cohen, L.F. Contributions to Hysteresis in Magnetocaloric Materials. *Phys. Status Solidi Basic Res.* **2018**, *255*, 2–9. [[CrossRef](#)]

32. Guo, L.; Lovell, E.; Wilson, N.; Burdett, P.; Cohen, L.F.; Ryan, M.P. The electrochemical behaviour of magnetocaloric alloys $\text{La}(\text{Fe,Mn,Si})_{13}\text{H}_x$ under magnetic field conditions. *Chem. Commun.* **2019**, *55*, 3642–3645. [[CrossRef](#)] [[PubMed](#)]
33. Wang, W.H.; Zheng, Z.G.; Huang, B.; Lai, J.W.; Zhou, Q.; Lei, L.; Zeng, D.C. Magnetocaloric effect, corrosion and mechanical properties of $\text{Mn}_{1.05}\text{Fe}_{0.9}\text{P}_{0.5}\text{Si}_{0.5}\text{Cu}_x$ alloys. *Intermetallics* **2019**, *113*, 106539. [[CrossRef](#)]
34. Hu, J.; Fu, S.; Huo, Y.; Long, Y.; Xue, J. Effect of impurity phase on corrosion resistance and magnetic entropy change for $\text{LaFe}_{11.3}\text{Co}_{0.4}\text{Si}_{1.3}\text{C}_{0.15}$ magnetocaloric compound. *J. Rare Earths* **2016**, *34*, 283–287. [[CrossRef](#)]
35. Zhu, F.; Lin, J.C.; Jiang, W.B.; Yang, C.; Li, L.F.; Zhang, X.K.; Song, W.H.; Zhu, X.B.; Tong, P.; Sun, Y.P. Enhanced mechanical properties and large magnetocaloric effect in epoxy-bonded $\text{Mn}_{0.98}\text{CoGe}$. *Scr. Mater.* **2018**, *150*, 96–100. [[CrossRef](#)]
36. Kavita, S.; Anusha, G.; Bhatt, P.; Suresh, V.; Vijay, R.; Sethupathi, K.; Gopalan, R. On the giant magnetocaloric and mechanical properties of Mn–Fe–P–Si–Ge alloy. *J. Alloys Compd.* **2020**, *817*, 153232. [[CrossRef](#)]
37. Zhang, H.; Sun, Y.; Niu, E.; Hu, F.; Sun, J.; Shen, B. Enhanced mechanical properties and large magnetocaloric effects in bonded $\text{La}(\text{Fe, Si})_{13}$ -based magnetic refrigeration materials. *Appl. Phys. Lett.* **2014**, *104*, 062407. [[CrossRef](#)]
38. Salas, F.H.; Mirabal-Garca, M. Quenching of the Hopkinson maximum under contamination in the system $\text{Gd}(0001)/\text{W}(110)$. *Phys. Rev. B* **1990**, *41*, 10859–10861. [[CrossRef](#)] [[PubMed](#)]
39. Morrish, A.H. *The Physical Principles of Magnetism*; Wiley: New York, NY, USA, 2001; ISBN 9780470546581.

Publisher’s Note: MDPI stays neutral with regard to jurisdictional claims in published maps and institutional affiliations.



© 2020 by the authors. Licensee MDPI, Basel, Switzerland. This article is an open access article distributed under the terms and conditions of the Creative Commons Attribution (CC BY) license (<http://creativecommons.org/licenses/by/4.0/>).